



**HAL**  
open science

## Deciphering human and climatic controls on soil erosion in intensively cultivated landscapes after 1950 (Loire Valley, France)

Anthony Foucher, Olivier Evrard, Olivier Cerdan, Clément Chabert, Irène Lefèvre, Rosalie Vandromme, Sébastien Salvador-Blanes

### ► To cite this version:

Anthony Foucher, Olivier Evrard, Olivier Cerdan, Clément Chabert, Irène Lefèvre, et al.. Deciphering human and climatic controls on soil erosion in intensively cultivated landscapes after 1950 (Loire Valley, France). *Anthropocene*, 2021, 34, pp.100287. 10.1016/j.ancene.2021.100287 . hal-03188433

**HAL Id: hal-03188433**

**<https://hal.science/hal-03188433v1>**

Submitted on 2 Apr 2021

**HAL** is a multi-disciplinary open access archive for the deposit and dissemination of scientific research documents, whether they are published or not. The documents may come from teaching and research institutions in France or abroad, or from public or private research centers.

L'archive ouverte pluridisciplinaire **HAL**, est destinée au dépôt et à la diffusion de documents scientifiques de niveau recherche, publiés ou non, émanant des établissements d'enseignement et de recherche français ou étrangers, des laboratoires publics ou privés.

# Anthropocene

## Deciphering human and climatic controls on soil erosion in intensively cultivated landscapes after 1950 (Loire Valley, France)

--Manuscript Draft--

<b>Manuscript Number:</b>	ANTHROPOCENE-D-20-00121R3
<b>Article Type:</b>	Research Paper
<b>Keywords:</b>	Intensive farming, Land use change, Soil degradation, Rainfall, Pond deposits, Computer Tomography scanner
<b>Corresponding Author:</b>	Anthony Foucher Gif sur Yvette, FRANCE
<b>First Author:</b>	Anthony Foucher
<b>Order of Authors:</b>	Anthony Foucher Olivier Evrard Olivier Cerdan Clément Chabert Irène Lefèvre Rosalie Vandromme Sébastien Salvador-Blanes
<b>Abstract:</b>	<p>The intensification of agricultural practices during the Anthropocene has induced an acceleration of soil erosion rates around the world. Although this phenomenon has been widely studied by means of monitoring or modelling at short timescales (&lt;10 years), few records are available for reconstructing this trajectory during longer periods (&lt;100 years). The analysis of sediment deposits in reservoirs was shown to provide a valuable tool for reconstructing this trend and identifying the driving factors disturbing the sediment cascade during the Anthropocene. Accordingly, sediment cores (n=5) were collected at the outlet of an intensively cultivated lowland catchment (24.5 km<sup>2</sup>, central France). These sedimentary sequences were dated using natural (<sup>210</sup>Pb<sub>ex</sub>) and artificial radionuclides (<sup>137</sup>Cs, <sup>241</sup>Am). The corresponding sediment accumulation and erosion rates were calculated for the 1928-2017 period. In addition, daily rainfall records, land use change and agricultural field patterns were reconstructed for the period comprised between the 1950s and 2017, based on weather chronicles, digitalized aerial images and agricultural census data. The results showed the substantial acceleration of erosion rates since 1928 (+500%). This increase occurred simultaneously with major landscape changes inducing an increase in plot size (+465%) and a decrease of the surface occupied by grassland and fallow land (-93%). Both parameters were shown to be highly correlated to the erosion rates reconstructed in this catchment (r=0.87 and r=0.95 for the plot size and grassland/fallow land surfaces, respectively). Between 1928 and 2017, erosion rates increased seven-fold in this lowland catchment. Although the long term trends of erosion are likely driven by landscape modifications, the current research has also demonstrated the major role played by rainfall intensity on the annual sediment dynamics.</p>

1 **Abstract**

2

3           Intensification of agricultural practices during the second half of the 20<sup>th</sup> century has accelerated  
4 of soil erosion around the world. Although this phenomenon has been widely investigated through a  
5 combination of monitoring or modelling at short timescales (<10 years), few records are available for  
6 reconstructing the trajectory of soil erosion during longer periods (i.e. the 20<sup>th</sup> century). Analysis of  
7 sediment deposits in reservoirs provides a valuable tool for reconstructing these trends and for  
8 identifying the driving factors that may have disturbed the sediment cascade after 1950. Accordingly,  
9 sediment cores (n=5) were collected in a reservoir located at the outlet of an intensively cultivated  
10 lowland catchment (24.5 km<sup>2</sup>) representative of those found in central France. Natural (excess lead-210)  
11 and artificial radionuclides (caesium-137, americium-241) enable dating of these sedimentary  
12 sequences. The corresponding sediment accumulation and erosion rates were calculated for the 1928-  
13 2017 period. In addition, daily rainfall records, land use change and agricultural field patterns were  
14 reconstructed for the period comprised between 1950 and 2017, based on weather records, digitalized  
15 aerial images (n=10) and agricultural census data (n=6). Results showed substantial acceleration of  
16 erosion rates after 1928 (+500%). This increase occurred simultaneously with major landscape changes  
17 that led to an increase in plot size (+465%) and decrease of the surface occupied by grassland and fallow  
18 land (-93%). Both parameters correlated strongly with the erosion rates reconstructed in this catchment  
19 (r=0.87 and r=0.95 for the plot size and grassland/fallow land surfaces, respectively). In addition,  
20 spectral analyses of daily rainfall records and mass accumulation rates, estimated with high temporal  
21 resolution from the sediment core tomography scanner data, showed concomitant short (i.e., 1 year) and  
22 long-term (i.e., 16 years) cycles between mass accumulation rates and rainfall. Overall, this study  
23 demonstrated the long-term impact of human activities and rainfall dynamics on soil erosion. Between  
24 1928 and 2017, erosion rates increased seven-fold in this lowland catchment, until reaching 31.5 t km<sup>-2</sup>  
25 yr<sup>-1</sup> by 2017. Although landscape modifications likely drove the pluri-decadal trends of erosion, this  
26 study has also demonstrated the major role played by rainfall intensity on annual sediment dynamics.

27

28 **Keywords:** Intensive farming, Land use change, Soil degradation, Rainfall, Pond deposits, Computer  
29 Tomography scanner, Sediment cascade

30

### 31 *1. Introduction*

32

33 Intensification of agricultural practices during the second half of the 20<sup>th</sup> century has induced  
34 widespread artificial terrestrial ecosystems (FAO, 2019). Between 1900 and 1960, ~ 40 million hectares  
35 were converted into arable land in Europe. At global scale, an average of 2.5 million hectares has  
36 converted each year into cultivated land between 1960 and 2015 (Klein Goldewijk et al., 2016). Major  
37 landscape modifications accompanied this global land conversion, with construction of artificial  
38 streams, ditches, drainage networks or the implementation of land consolidation operations (e.g. Chartin  
39 *et al.*, 2013; Vandromme *et al.*, 2013). These landscape modifications have allowed significant increase  
40 of the size of the plot and the surface area occupied by agricultural land at the expense of wetland,  
41 woodland and dryland.

42 The implementation of these modern agricultural practices associated with the widespread use of  
43 agrochemicals after 1950 has significantly increased the cereal production yields (multiplied by 3  
44 between 1960 and 2015, FAOSTAT). It has also induced multiple detrimental effects, however, on  
45 terrestrial ecosystems and river systems (Boardman and Poesen, 2006; Issaka and Ashraf, 2017). Among  
46 other impacts, the acceleration of soil erosion disturbed the sediment cascade by modifying the transport  
47 of sediment across the landscape. These disturbances have generated deleterious impacts in response to  
48 this increased sediment delivery (e.g. de Vente *et al.*, 2007), including the accelerated transport of  
49 pollutants (e.g. Evrard *et al.*, 2016) or the loss of aquatic biodiversity (e.g. Wantzen, 1998). Nowadays,  
50 the global loss of soil was estimated to 43 Pg.yr<sup>-1</sup> and it may further increase by 30 to 66% in 2070,  
51 according to the latest climate forecast projections (Borrelli et al., 2020).

52 Soil conservation has been recognized by the United Nations as one of the main challenges of  
53 the 21<sup>st</sup> century (Amundson et al., 2015; Robinson et al., 2017). To better manage soils, identifying the  
54 main factors controlling erosion (i.e. climate and/or land use change) is essential to limit potential  
55 deleterious impacts on terrestrial and aquatic ecosystems (Evrard et al., 2010). A major obstacle to

56 anticipate the future impacts of climate and land use changes on the global sediment cascade is the lack  
57 of long-term monitoring records (Dearing and Jones, 2003). In general, studies focusing on soil erosion  
58 are based on global modeling (García-Ruiz et al., 2015; Maetens et al., 2012), local plot studies (Chaplot  
59 and Le Bissonnais, 2000) or catchment monitoring during a few years (Grangeon et al., 2017;  
60 Vanmaercke et al., 2011). These methods provide valuable information on sediment delivery during the  
61 most recent period (i.e post-1990s). Investigating the human impact on sediment delivery, however,  
62 requires information on process-response mechanisms that take place over timescales that exceed a few  
63 decades. These periods are considerably longer than the common duration of river monitoring  
64 programmes (Dearing and Jones, 2003). As an alternative, analysis of sediment archived in lakes and  
65 artificial reservoirs may offer opportunity to reconstruct pre- and post-impact soil erosion trajectories  
66 and their response to forcing factors over longer periods. This methodology was successfully applied  
67 under various climate conditions (Dearing, 1991; Foster et al., 2011; Gellis et al., 2006) and over  
68 different timescales ( $10^0$  years to  $10^3$  years), (Bajard et al., 2015; Verstraeten and Poesen, 2002).  
69 Previous research conducted on these natural archives has demonstrated the impact of climate and  
70 human activities on sediment delivery (Foster and Walling, 1994). It has also outlined that sedimentary  
71 sequences generally record the result of both processes. As an example, Foster *et al.* (2003a) highlighted  
72 in an Alpine sedimentary sequence that climate fluctuations controlled sediment delivery on short  
73 timescales ( $10^0$ - $10^2$  years), whereas land use changes controlled major changes in sediment supply over  
74 timescales ranging between  $10^2$  and  $10^3$  years. Consequently, the use of independent historical  
75 information regarding the timing and the magnitude of climatic and anthropogenic forcing factors is  
76 required to demonstrate the respective impact of both types of factors on sediment delivery throughout  
77 time (Dearing and Jones, 2003; Schiefer et al., 2013). According to Mitchell & Hulme (1999), future  
78 assessments of sediment delivery must deal with both uncertain human and climate forcing factors and  
79 explore small catchments, which are more responsive to impacts and show the largest changes in  
80 sediment delivery (Dearing and Jones, 2003). Although investigations of sediment transfer has been  
81 widespread in highland areas based on cores collected in lakes and reservoirs, few studies have taken  
82 place in lowland areas although these regions were highly impacted by the intensification of agricultural  
83 practices during the 20<sup>th</sup> century. Furthermore, studies have rarely compared these sedimentary

84 reconstructions with historical archives on land use change (Foucher et al., 2019b) or rainfall chronicles  
85 (Foucher et al., 2019a) for identifying the main driving factors among climatic and anthropogenic  
86 pressures, since historical databases are rarely available over several decades.

87 In this study, we collected sediment cores in a pond draining a small (24.5 km<sup>2</sup>) and intensively  
88 cultivated lowland catchment located in central France, representative of the intensive agricultural areas  
89 found across Northwestern Europe. To improve knowledge on soil erosion dynamics over the post-1950  
90 period, we addressed the following questions: (1) What is the trajectory of soil erosion and sediment  
91 delivery in lowland intensively cultivated catchments during the 20<sup>th</sup> century? ; (2) What were the main  
92 factors controlling erosion in this environment during this period?

93

94 We hypothesized that more intensive rainfall and the intensification of agricultural practices have  
95 accelerated soil erosion and sedimentation rates during the 20<sup>th</sup> century. To test this hypothesis, we  
96 conducted a multi-proxy paleolimnological study based on the characterization of terrigenous and  
97 organic sediment fractions in lacustrine archives dated with fallout radionuclide analyses. We further  
98 compiled historical archives on land use change and rainfall chronicles to shed light on the respective  
99 contribution of climate and land use on post-1950 erosion, and therefore links between erosion  
100 dynamics, land use and climate variability.

101

## 102 *2. Study site and methods*

103

### 104 *2.1 Study site*

105 The Brosse site (47.275566N, 1.055248E) is a small headwater catchment (24.5 km<sup>2</sup>) located in  
106 the middle part of the Loire River basin (117,000 km<sup>2</sup>), one of the most intensively cultivated areas of  
107 central France (Fig. 1). This catchment is characterized by a gentle topography (elevation ranges  
108 between 80 and 130 m a.s.l with an average slope of 1.1%) and by an oceanic climate (average annual  
109 rainfall of 677 mm). Three geological units dominates the geology of this area: Secondary flint clays  
110 (*formations argilo-siliceuses* - Lower and Middle Senonian) in the northeastern part of the catchment  
111 are composed of white or greenish clays dominated by smectites or kaolinites enriched in flint (deposits

112 have a variable thickness of 2 to 3 m). A dominant Tertiary calcareous unit (*Calcaire de Touraine –*  
113 *Eocene-Oligocene*) overlies this unit, shaping a plateau incised by erosion (maximal thickness of 20m)  
114 partly covered with some residual Quaternary silt deposits with a variable thickness rarely exceeding  
115 0.5 to 1.5 m (Rasplus et al., 1982). As a result, soils are mostly calcareous, partly leptochreous Cambisols as  
116 well as hypereutric Cambisols developed on Tertiary deposits, and to a lesser extent Cambisols and luvisol  
117 Cambisols developed on more recent deposits (Boutin and Thomas, 1987; FAO, 2006).

118 This lowland basin is exclusively devoted to intensive agriculture. Arable land (84%), and to a  
119 lesser extent forest (11%) and rural settlements (4%), dominates the current land use. According to the  
120 agricultural census available since 1955, this land use distribution has not significantly changed during  
121 the second half of the 20<sup>th</sup> century (Fig. 2 & Fig. S1). Nevertheless, increasing the sizes of plots and  
122 installing irrigation systems have changed the landscape since 1950.

123 The catchment river's network (approximately 15.5 km long) drains into a pond created during  
124 the 16<sup>th</sup> century. This shallow water body of 11 ha has an average depth of 1 m with a maximal depth of  
125 2.4 m close to the dam, in the northern part of the pond (Fig. 1).

126

## 127 2.2 Material and methods

128

### 129 2.2.1 Limnological approaches

130 Sediment cores (n=5, with lengths ranging between 65 and 127 cm) were collected in 2017  
131 along two cross-sections (NE-SO and NO-SE) in the Brosse pond using a floating platform and a Uwitec  
132 gravity corer equipped with a 90mm PVC liner (Fig. 1). We chose the location of these cores to  
133 document potential variations of sediment dynamics across the reservoir based on the pond bathymetry  
134 and the sediment thickness. A Garmin *Echomaps* depth sounder provided bathymetric data, core  
135 locations and the thickness of sediment. We conducted most analyses on the master core BR-05 that  
136 allowed the longest temporal reconstruction. We used other cores to characterise the heterogeneity of  
137 sediment accumulation rates across the pond, as well as to quantify the volume of sediment accumulated  
138 in the reservoir.

139

140 *Non-destructive laboratory analyses*

141 An Avaatech core scanner (EPOC Laboratory, Bordeaux University, France) enabled X-ray  
142 fluorescence (XRF) measurements. High-density records (with a 0.5mm resolution) provided relative  
143 information on the sediment geochemical content (expressed in counts by second (cps)). The  
144 calcium/titanium (Ca/Ti) ratio was calculated for characterizing the biogenic/detrital ratio (Croudace  
145 and Rothwell, 2015). These high-resolution values were calibrated using point-based measurements of  
146 Total Organic Carbon (OC) for estimating along the entire sequence the proportions of terrigenous and  
147 organic sediment fractions accumulated throughout time. We used the volume of the terrigenous  
148 fraction accumulated in the reservoir for reconstructing soil erosion rates.

149 Non-calibrated sediment density was recorded every 0.6 mm along the sediment sequences  
150 using Computer Tomography scanner (CT-scan) images obtained using the equipment (Siemens  
151 Somatom 128 Definition AS scanner) available at the CIRE platform (Surgery and Imaging for Research  
152 and Teaching; INRA Val de Loire, France).-Relative density values (CT-number) were extracted from  
153 the scanner images using the free software ImageJ (Schneider et al., 2012) and were calibrated by  
154 measuring the absolute dry bulk density ( $\text{g}\cdot\text{cm}^{-3}$ ) in samples collected randomly along the cores (n=290).  
155 Density values enabled quantification of the volume of sediment accumulated in the reservoir by  
156 converting the sedimentation rates into mass accumulation rates.

157

158 *Destructive laboratory analyses*

159 Particle size analyses were undertaken following 1 cm depth increments in the five cores using  
160 a laser diffraction Malvern Mastersizer 3000 grain-sizer (allowing theoretically measurements on  
161 particles with diameters comprised between 0.01 and 3500  $\mu\text{m}$ ).

162 We measured the concentration in carbonates in 10 samples selected on the master core (with  
163 a Bernard calcimeter (University of Tours, France) following the method described in NF ISO 10693  
164 (1995). When detected, we removed carbonates from these samples before performing Isotope Ratio  
165 Mass Spectrometer analyses (IRMS). On these decarbonized samples, IRMS analyses were conducted  
166 on dry sediment for elemental (Total Organic Carbon (OC) and Total Nitrogen (TN)) and stable Carbon  
167 and Nitrogen isotopes ( $\delta^{13}\text{C}$ ,  $\delta^{15}\text{N}$ ) measurements. We performed these measurements with a continuous

168 flow Elementar® VarioPyro cube analyzer coupled to a Micromass® Isoprime IRMS at the Institute of  
169 Ecology and Environmental Science of Paris, France. Stable and elemental isotopes were used in  
170 addition to the Ca/Ti ratio for identifying the sources of organic carbon (autochthonous versus  
171 allochthonous) accumulated in the reservoir.

172

### 173 *Core chronology*

174 Gamma spectrometry enabled establishment of the age control of the master core (BR-05), (Fig.  
175 3). Two complementary radioisotopes are classically analyzed. The Caesium-137 ( $^{137}\text{Cs}$ ) is used as a  
176 discrete time marker that provides anchoring points after 1950. In contrast, Lead-210 ( $^{210}\text{Pb}_{\text{ex}}$ ) is used  
177 as a continuous time marker to reconstruct sedimentation rates for the last 100 to 150 years.  $^{210}\text{Pb}_{\text{ex}}$  and  
178  $^{137}\text{Cs}$  activities were obtained on 19 samples (~15g of dried sediment) collected along the core using the  
179 very low background GeHP detectors available at the Laboratoire des Sciences du Climat et de  
180 l'Environnement (Gif-sur-Yvette, France). Activities were decay-corrected to the sampling date (Evrard  
181 *et al.*, 2016).

182 We determined continuous ages taking into account the exponential decay of  $^{210}\text{Pb}_{\text{ex}}$  and the  
183 application of the Constant Rate of Supply model, (Appleby and Oldfield, 1978). This model assumes  
184 variations in the rate of sediment accumulation with a constant rate of unsupported Lead-210 from  
185 atmospheric fallout. We performed validation of the age model using  $^{137}\text{Cs}$  as a time marker. This  
186 artificial radionuclide may originate from two sources in Western Europe: the peak of thermonuclear  
187 weapon testing (maximal emission in 1963) and the Chernobyl accident (1986). To distinguish between  
188 both potential  $^{137}\text{Cs}$  sources, Americium-241 ( $^{241}\text{Am}$ ) was used to identify the  $^{137}\text{Cs}$  peak attributed to  
189 the maximum nuclear bomb fallout (e.g. Cambray *et al.*, 1989).

190 We obtained age models of the other cores after correlation with the master core using XRF and  
191 CT-Scan data.

192

### 193 *From sediment dynamics to erosion rates*

194 We estimated mass Accumulation Rate (MAR, expressed in  $\text{g cm}^{-2} \text{yr}^{-1}$ ) for each individual core  
195 using the Sediment Accumulation Rate (SAR,  $\text{cm yr}^{-1}$ ), the Dry Bulk Density (DBD, expressed in  $\text{g cm}^{-3}$   
196 and extracted from the calibrated tomography scanner CT-number) following equation 1 (eq. 1). The  
197 MAR corresponds to the amount of material deposited at each individual coring site. This sediment is a  
198 mixture of material originating from terrestrial inputs (allochthonous inputs) and material directly  
199 produced in the water body (autochthonous production).

200

201 (eq. 1)  $\text{MAR} [\text{g cm}^{-2} \text{yr}^{-1}] = \text{DBD} [\text{g cm}^{-3}] \times \text{SAR} [\text{cm yr}^{-1}]$

202

203 We estimated the rates of organic and terrigenous matter deposition with the Mass  
204 Accumulation Rate of organic (MARorg) and minerogenic sediment (MARmin) calculated as follows:

205

206 (eq. 2)  $\text{MAR}_{\text{org}} [\text{gC cm}^{-2} \text{yr}^{-1}] = \text{DBD} [\text{g cm}^{-3}] \times \text{SAR} [\text{cm yr}^{-1}] \times \text{TOC} [\text{gC g}^{-1}]$

207 (eq. 3)  $\text{MAR}_{\text{min}} [\text{g cm}^{-2} \text{yr}^{-1}] = \text{MAR} [\text{g cm}^{-2} \text{yr}^{-1}] - \text{MAR}_{\text{org}} [\text{gC cm}^{-2} \text{yr}^{-1}]$

208

209 We reconstructed the volume of sediment deposited in the Brosse pond by multiplying the MAR  
210 of each individual core with the area of influence around the corresponding cores. These influence  
211 polygons were automatically computed with the free software QGIS according to the reservoir  
212 bathymetry and the distance between the cores based on the Thiessen polygons method. To obtain the  
213 corresponding volume of organic and minerogenic matter accumulated in the reservoir, the influence  
214 surface areas were multiplied with the MARorg and MARmin. During the 20<sup>th</sup> century, the pond surface  
215 has potentially changed inducing an evolution in the surface areas of the influence polygons. For  
216 reducing errors associated with these surface variations, the pond shape was digitized using 10 aerial  
217 images collected between 1950 and 2017.

218 Verstraeten and Poesen (2000) demonstrated the importance of calculating the trapping  
219 efficiency for correcting the volume of sediment accumulated in small ponds. This parameter  
220 corresponds to the proportion of deposited or trapped sediment coming into a reservoir. This estimation

221 requires the suspended-load measurements conducted upstream/downstream of the dam or at both  
222 locations. In this research, as in most previous studies (e.g. Ben Slimane *et al.*, 2013), these data were  
223 not available because of the lack of gauging stations on river networks draining agricultural  
224 environments. The outlet of the Brosse reservoir has an elongated shape with the absence of overflows  
225 during the winter period. In addition, according to local inhabitants, the scour valve for sediment  
226 flushing from the reservoir has not been used during the last century. Intermittent flow characterises the  
227 drainage network, and water in the pond is clear during low stage periods. Given the absence of  
228 overflows, all sediment originating from the catchment was considered to have been trapped in the  
229 Brosse reservoir.

230 We calculated the minimal erosion rate ( $\text{t km}^{-2} \text{ yr}^{-1}$ ) by multiplying the volume of the minerogenic  
231 sediment fraction with the catchment surface area. As the origin of organic matter was indiscriminable  
232 between the respective contributions of primary productivity or terrigenous sources (e.g. Simonneau *et*  
233 *al.*, 2013), we calculated the maximal value of erosion by multiplying the volume of both minerogenic  
234 and organic sediment fractions with the catchment surface area.

235

### 236 2.2.2 Evolution of land use

237

238 We reconstructed past changes in land use and plot size based on digitized aerial images and on  
239 statistical records available from the French agricultural census. We digitized images taken in the Brosse  
240 catchment during ten aerial surveys conducted between 1950 and 2011 (respectively in 1950, 1972,  
241 1981, 1989, 1991, 1995, 1997, 2002, 2007 and 2011). Five main land uses on the images were  
242 documented: forests, water bodies, urban settlements, arable land and grassland/fallow land. In addition,  
243 agricultural census data available between 1950 and 2010 (respectively in 1950, 1970, 1979, 1988, 2000  
244 and 2010) enabled reconstruction of the evolution of dominant crop types (e.g. wheat, barley, corn, rape,  
245 sunflower, ...), as well as the surface areas occupied by permanent and temporary grassland, and fallow  
246 land. To supplement this information, we reconstructed major landscape management operations  
247 implemented in the catchment during the 20<sup>th</sup> century based on historical information provided in a

248 database of the Regional Department of Agriculture (land consolidation, stream re-design, tile drain  
249 implementation).

250

### 251 2.2.3 Rainfall variability

252

253 We extracted daily rainfall information from the SAFRAN climate database (Système  
254 d'Analyse Fournissant des Renseignements Adaptés à la Nivologie) produced by the official French  
255 meteorological agency (Météo France) and available since 1959 according to a 8-km resolution grid.  
256 This database provided cumulative daily rainfall values. Merging These data generated monthly and  
257 annual cumulative rainfall.

258

### 259 2.2.4 Statistical treatment

260

261 We used the Mann–Kendall non-parametric test (MK-test) for detecting monotonic upward or  
262 downward trends of a given variable (MAR, volume of sediment, rainfall) throughout time (with a P-  
263 value level of 0.05), (Warren and Gilbert, 1988).

264 We performed spectral analysis based on a simple periodogram on rainfall data with the free  
265 software PAST3 (Hammer et al., 2001). This procedure enabled identification of the occurrence of  
266 cyclicity in time series data. This analysis is based on the Lomb periodogram algorithm for unevenly  
267 and evenly data. The spectrum analysis was performed with a significant level  $<0.01$ .

268

269

## 270 3. Results

271

### 272 3.1 Evolution of land use and land cover

273

274 During the 1950-2010 period, the number of plots found in the Brosse catchment decreased by  
275 83%, from 3100 to 550 plots (Fig. 2B). The fastest decline occurred between 1950 and 1972 (decrease

276 of 60% of the plot number) whereas smaller changes were recorded after 1972 (+4%), 1981 (-30%) and  
277 1989 (-23%). From 1995 to 2010, the number of plots has remained constant. Following this general  
278 decrease between 1950 and 2010, the average size of the plots increased by 465% from an average of  
279 0.6 ha in 1950 to 3.6 ha in 2010.

280 According to the digitized aerial images, the main land uses have not significantly changed in  
281 the catchment during the second half of the 20<sup>th</sup> century (Fig. 2A). In 1950, the forest and urban areas  
282 occupied respectively 14.3% and 3.5% of the catchment surface while cultivated land covered  
283 approximately 82.5% of the total catchment area. In 2010, these proportions amounted to 10.6%  
284 (forests), 4.3% (urban areas) and 84% (cultivated land) of the surface. Whilst no significant change in  
285 the arable land surface proportion was evident in this catchment, the types of agricultural land cover  
286 have undergone major changes since 1950. According to the agricultural census, the surface occupied  
287 by grassland/fallow land decreased by 93% during the second half of the 20<sup>th</sup> century (from 27% of the  
288 surface in 1955 to 2% in 2010). This land cover proportion started to decrease after 1965 (when it  
289 covered 30% of the catchment surface) before stabilizing in 1995 (amounting to 4% of the catchment  
290 surface). Grassland and fallow land declines in this catchment are highly correlated to the decrease in  
291 the number of individual plots ( $r=0.86$ ). According to the agricultural census data, surfaces devoted to  
292 permanent and temporary grassland as well as fallow land were mainly converted into winter and spring  
293 crops.

294 Both changes in plot size and land use/cover occurred during a period of major management  
295 operations in this catchment. Between 1950 and 2010, land consolidation programmes were conducted  
296 in 1960, 1964, 1971, 1987, 1998 and 2006. In addition to these major operations, two reservoirs appeared  
297 in 1977 and in 1991 for irrigation purposes. The latest pond is located in the southeastern part of the  
298 catchment (Fig. 1). Its creation led to the increase in the surface occupied by water bodies in the Brosse  
299 catchment by 107% (from 13ha before 1991 to 24ha afterwards). The creation of these artificial dams  
300 has induced a decrease of the catchment size directly connected to the Brosse pond. The corresponding  
301 surface area decreased from 24.5 km<sup>2</sup> before 1977 to 21.5 km<sup>2</sup> in 1991 and even to 13.9 km<sup>2</sup> in 2017.

302

303

### 304 3.2 Chronology and core description

305

306 The lowest layers in the core BR-05 where  $^{137}\text{Cs}$  activities could be detected were found between  
307 96 and 97 cm ( $2.1 \text{ Bq.kg}^{-1}$ , SD  $0.3 \text{ Bq.kg}^{-1}$ ) with a maximal activity recorded at 92.5cm depth ( $27.6$   
308  $\text{Bq.kg}^{-1}$ , SD  $0.4 \text{ Bq.kg}^{-1}$ ). No radiocesium peak associated with the 1986 fallout was clearly visible in  
309 this sedimentary sequence (Fig. 3). Maximal  $^{137}\text{Cs}$  activities were associated with the detection of  $^{241}\text{Am}$   
310 ( $0.5 \text{ Bq.kg}^{-1}$ , SD  $0.1 \text{ Bq.kg}^{-1}$ ). This level was therefore attributed to the 1963 fallout.

311 Activities in  $^{210}\text{Pb}_{\text{ex}}$  decreased according to a linear regression ( $r^2=0.95$ ), (activities ranged between 36  
312 and  $7 \text{ Bq.kg}^{-1}$  from the top to the bottom of the core), (Fig. 3). Application of the CRS age model allowed  
313 detection of the radiocesium time markers at the expected levels ( $\pm$  one year). The lowest occurrence of  
314  $^{137}\text{Cs}$  activities in this sedimentary sequence (97 cm depth) was dated to 1957 and the base of the core  
315 was dated to 1928 (127 cm depth). Radionuclide data are provided in Table 1.

316 The 127 cm length of the Brosse sedimentary sequence (BR-05) was composed of three main  
317 units. The first unit ranging between 1 and 80 cm depth (respectively between 2017 and 1972) was  
318 characterized by fine homogenous deposits (average  $d_{50} = 16 \mu\text{m}$ , SD  $2 \mu\text{m}$ ) dominated by terrigenous  
319 material (92.8%, SD 0.8%), (Fig. 4). Organic material deposited during this period showed a C:N ratio  
320 ranging between 7.8 and 8.6. The second unit located between 80 and 114 cm depth (1972-1943 period)  
321 was composed of more heterogeneous and coarser material (average  $d_{50} = 43 \mu\text{m}$ , SD  $14 \mu\text{m}$ ) with a  
322 greater proportion of organic matter (12.9%, SD 4.4%), (Fig. 4). The highest proportion of organic  
323 material of the Brosse master core was recorded in 1962 (25% of organic material). This unit 2 was  
324 characterized by a C:N ratio ranging between 8.6 and 10.7. Finally, the last unit was found between 114  
325 and 127 cm depth (respectively between 1943 and 1928). This unit was made of fine grey material  
326 (average  $d_{50} = 25 \mu\text{m}$ , SD  $19 \mu\text{m}$ ) mainly composed of minerogenic sediment (95%, SD 1.8%), (Fig.  
327 4).

328

### 329 3.3 Mass accumulation rates

330

331 The occurrence of two main periods characterized the MAR of the master core BR-05. The first  
332 period is characterized by a constant delivery of sediment between 1928 and 1960 (average value of 392  
333  $\text{g m}^{-2} \text{ yr}^{-1}$ , SD  $35 \text{ g m}^{-2} \text{ yr}^{-1}$ ). An acceleration of sediment delivery (average value of  $564 \text{ g m}^{-2} \text{ yr}^{-1}$ , SD  
334  $80 \text{ g m}^{-2} \text{ yr}^{-1}$ ) marked the second period between 1960 and 2017. On this statistical positive linear trend  
335 ( $r^2=0.7$ ), (MK test  $p$ -value  $<0.01$ ), a peak was recorded between 1964 and 1968 (maximum value of  
336 sediment accumulation rate of  $580 \text{ g m}^{-2} \text{ yr}^{-1}$  in 1968).

337 We estimated the proportions of MAR<sub>min</sub> and MAR<sub>org</sub> using the high correlation observed  
338 between the continuous Ca/Ti XRF ratio and the punctual TOC contents ( $r^2=0.96$ ). Both MAR<sub>min</sub> and  
339 MAR<sub>org</sub> displayed a positive trend during the 1928-2017 period (MK test  $p$ -value  $<0.01$ ), (Fig. 4).  
340 Rates of accumulation of mineral matter remained constant between 1928 and 1960 with an average  
341 value of deposition of  $352 \text{ g m}^{-2} \text{ yr}^{-1}$  (SD  $36 \text{ g m}^{-2} \text{ yr}^{-1}$ ). From 1960 to 2017, the rate of MAR<sub>min</sub>  
342 increased according to a linear trend ( $r^2=0.74$ ) from  $370$  to  $640 \text{ g m}^{-2} \text{ yr}^{-1}$  (respectively in 1960 and 2017).  
343 The MAR<sub>org</sub> showed a constant value between 1928 and 1940 ( $17.5 \text{ gC m}^{-2} \text{ yr}^{-1}$ , SD  $5 \text{ gC m}^{-2} \text{ yr}^{-1}$ ). The  
344 highest rate of organic matter deposition was recorded during the 1940-1970 period, with an average  
345 value of  $57 \text{ gC m}^{-2} \text{ yr}^{-1}$  (SD  $18 \text{ gC m}^{-2} \text{ yr}^{-1}$ ). During this period, two maxima were recorded between  
346 1945 and 1949 (maximal value of  $61 \text{ gC m}^{-2} \text{ yr}^{-1}$  in 1948) and between 1958 and 1967 (maximal value  
347 of  $114 \text{ gC m}^{-2} \text{ yr}^{-1}$  in 1962) - (Fig. 4). After 1970, MAR<sub>org</sub> increased according to a linear trend ( $r^2=0.85$ )  
348 from  $32 \text{ gC m}^{-2} \text{ yr}^{-1}$  in 1970 to  $56 \text{ gC m}^{-2} \text{ yr}^{-1}$  in 2017.

349

350

### 351 3.4 Reconstructing soil erosion rates

352

353 The surface area of the Brosse pond has significantly changed during the second half of the 20<sup>th</sup>  
354 century increasing from an average of  $3.8 \text{ ha}$  (SD  $0.6 \text{ ha}$ ) between 1950 and 1965 to  $10.4 \text{ ha}$  (SD  $0.9 \text{ ha}$ )  
355 between 1968 and 2017. The increase of the reservoir surface between 1965 and 1968. Even when taking  
356 into account this change in surface area of the pond, the volume of sediment accumulated in the reservoir  
357 showed a statistically significant increasing trend with time during the 20<sup>th</sup> century (MK test  $p$ -value  
358  $<0.01$ ), (Fig. 5). Between 1925 and 1955,  $135 \text{ t.yr}^{-1}$  (SD  $4 \text{ t.yr}^{-1}$ ) of sediment accumulated on average.

359 Minerogenic material (in average  $125 \text{ t.yr}^{-1}$ , SD  $4 \text{ t.yr}^{-1}$ ) dominated sediment inputs (Fig. 5). From 1955  
360 to 1990, the quantity of sediment deposited increased considerably from 155 to  $540 \text{ t.yr}^{-1}$ . During this  
361 period, minerogenic sediment remained the main source of material accumulated in the pond (90%, SD  
362 5%). After 1990, the amount of material deposited decreased by 39% (corresponding to a volume of  $375$   
363  $\text{t.yr}^{-1}$ ) due to the construction of a secondary dam in the southeastern part of the catchment inducing a  
364 35% decrease of the area draining into the Brosse pond (Fig. 1). Finally, from 1995 to 2017, the volume  
365 of sediment accumulated in the reservoir increased again from 435 to  $475 \text{ t.yr}^{-1}$  (Fig. 5).

366 The reconstruction of erosion rates shows a similar trajectory as that of sediment accumulation  
367 with an acceleration of erosion processes after 1960 (Fig. 5). Between 1925 and 1955, mean erosion  
368 rates of  $5.5 \text{ t km}^{-2} \text{ yr}^{-1}$  (SD  $0.2 \text{ t km}^{-2} \text{ yr}^{-1}$ ) were recorded. From 1960, a linear increasing trend ( $r^2=0.86$ )  
369 was observed. During this period, erosion rates increased from 5.3 (SD  $1 \text{ t km}^{-2} \text{ yr}^{-1}$ ) to  $31.5 \text{ t km}^{-2} \text{ yr}^{-1}$   
370 (SD  $(2.8 \text{ t km}^{-2} \text{ yr}^{-1})$ ), (respectively between 1960 and 2017). We recorded two peaks of erosion intensity  
371 between 1980-1985 and 1995-2000 ( $26.5$  and  $29.4 \text{ t km}^{-2} \text{ yr}^{-1}$ ), respectively. From the 1925-1930 period  
372 to the end of the Brosse sedimentary sequence in 2017, erosion rates further increased by 520%.

373

374

### 375 3.5 Rainfall and sediment delivery

376

377 During the 1959-2017 period, annual rainfall ranged between 360 and  $830 \text{ mm yr}^{-1}$  with an  
378 average value of  $630 \text{ mm yr}^{-1}$  (SD  $107 \text{ mm yr}^{-1}$ ). The driest year was in 2005 whereas the most humid  
379 year occurred in 1994. According to the MK test, no statistical trend in rainfall was evident during the  
380 studied period (MK test  $p$  value  $> 0.7$ ). The spectral analysis of daily rainfall monitored between 1959  
381 and 2017 underlined the occurrence of five cyclicities with a  $p$  value  $< 0.01$  recorded respectively every  
382 16.3 years and every 365, 182, 24 and 15 days (Fig. 6).

383 We conducted spectral analysis on the high resolution MAR values after removing the long-  
384 term trend. These results suggested occurrence of eight cyclicities with  $p$  value  $< 0.01$  between 1960  
385 and 2017. These cyclicities occurred every 28.5, 15.2, 11, 8.8, 6.3, 3, 2.6 and 1.2 years. During this

386 period, the maximal values of MAR appeared recorded in 1960, 1967 and 1980. The minimal values  
387 were identified in 1977, 2009 and 2016 (Fig. 6).

388 A correlation coefficient ( $r^2$ ) of 0.4 was observed between monthly rainfall and estimated monthly MAR  
389 values after removing a linear trend that was likely associated with sediment consolidation between  
390 January and December 2016 corresponding to the well-dated top core. This relationship was, however,  
391 less clear during the 1960-2017 period ( $r^2 < 0.1$ ).

392

393

#### 394 4. Discussion

395

396 The major increase of soil erosion during the 20<sup>th</sup> century recorded in the Brosse reservoir started  
397 after the first land consolidation operations conducted successively in 1960, 1964 and 1971. These  
398 management operations occurred simultaneously with increase of the erosion rates (+80% in 11 years).  
399 This acceleration of soil erosion is characterized in the Brosse pond by a change in organic matter  
400 sources (Foucher et al., 2020), (Fig. 4). The increase in C:N ratio observed during this period suggested  
401 the dominant delivery and accumulation of organic material originating from terrigenous sources  
402 (Meyers, 1994). In addition, the highest  $^{137}\text{Cs}$  activities recorded between 1960 and 1978 can be  
403 associated with the 1963 radiocesium fallout, but it may also indicate the occurrence of a period of  
404 erosion characterized by a greater contribution of surface sources (i.e. upper tilled soil layer), (Evrard et  
405 al., 2020). This acceleration of sediment terrigenous inputs in the Brosse pond after 1950 was also  
406 observed in other European countries as well as in Japan and in North America (Ahn et al., 2010; Foster  
407 and Walling, 1994; Heathcote et al., 2013).

408 The second period of increase in soil erosion in the Brosse pond after 1970 (Fig. 5) coincided  
409 with a phase of major land use change. Between 1970 and 1985, 72% of the fallow land, temporary and  
410 permanent grassland were converted into cropland without affecting the size of the plots (Fig. 2). These  
411 changes in land cover accelerated soil erosion, which increased by 107% from 12.5 to 26.5 t km<sup>-2</sup> yr<sup>-1</sup>  
412 between 1970 and 1985 (Fig. 5). This period was also characterized by a limited decrease of the C:N  
413 ratio, suggesting a greater contribution of autochthonous organic matter, particularly after 1980 (Fig. 4).

414 This observation was confirmed by an increase of the chlorophyll-a signature from this period onwards  
415 (Foucher et al., 2020). This change in organic matter sources can be attributed to the widespread use of  
416 synthetic fertilizers in this catchment, as observed across the entire Loire River basin (Poisvert, 2018)  
417 inducing a greater algal production in the reservoir.

418 These results further demonstrate the impact of changes in land use and agricultural practices on soil  
419 erosion, consistent with previous studies (e.g. Bakker *et al.*, 2008) and in particular in Holocene  
420 sedimentary sequences (e.g. De Boer, 1997; Giguët-Covex *et al.*, 2014).

421 In contrast, the decrease in sediment deposition during the last three decades (1990-2017) in the  
422 Brosse reservoir occurred just after the creation of an artificial dam (1991). The dam likely trapped  
423 sediment originating from the southeastern part of the catchment. During this period, however, soil  
424 erosion continued to increase by 26% (respectively from 25.4 to 31.5 t km<sup>-2</sup> yr<sup>-1</sup> between 1990 and 2017),  
425 (Fig. 5). This acceleration occurred during the last land consolidation operations that were respectively  
426 conducted in 1998 and 2006. Between 1990 and 2007, the number of plots decreased by 40% (from 724  
427 plots in 1989 to 440 plots in 2007), (Fig. 4). The organic matter accumulated in the pond between 1990  
428 and 2017 was characterized by the lowest C:N ratios observed along the entire sedimentary sequences,  
429 as well as by the highest chlorophyll-a concentration (Foucher et al., 2020), reflecting an increase of  
430 primary productivity due to enhanced nutrient inputs.

431 When comparing the detailed history of land use change and landscape management with the  
432 evolution of soil erosion rates reconstructed from the pond records between 1928 and 2017, two potential  
433 driving factors of erosion may be identified in this intensively cultivated catchment: the decrease of the  
434 number of plots and the changes in land cover and agricultural practices. Both factors are highly  
435 correlated with erosion rates ( $r^2= 0.87$  respectively for erosion *versus* plots number and  $r^2= 0.95$  for  
436 erosion *versus* grassland /fallow land surfaces), (Fig. 7). Other additional factors such as widespread use  
437 of herbicides (Sabatier et al., 2021) or changes in cultivated species may also have affected the rates of  
438 soil erosion (Mann et al., 2002) during the last several decades. In the absence of detailed information  
439 on these parameters, they were not further taken into account in this discussion.

440 Beyond this long term relationship between landscape modifications and erosion, the high  
441 resolution MAR values obtained after removing the linear trend probably associated with the sediment

442 consolidation allowed the identification of an annual cyclicity (1.2 year) as well as a longer cyclicity  
443 feature (15.2 years) similar to that observed for rainfall data (1 year and 16.3 years, respectively). The  
444 CT-scan method was already successfully applied for identifying climatic oscillations in Holocene  
445 sedimentary sequences (St-Onge and Long, 2009). The annual and inter-decadal frequency records  
446 observed in this study were also widely identified in meteorological data across Europe (e.g. Germany,  
447 Marković & Koch (2005)). These results suggest that, in addition to the main driving factor attributed  
448 to human activities, the Brosse sedimentary sequence and the associated MAR fluctuations recorded the  
449 impact of annual and multi-decadal rainfall oscillations. The impact of rainfall was one of the main  
450 factors controlling soil erosion rates (Römkens et al., 2002). This relationship is often documented based  
451 on records available at river monitoring stations (e.g. Grangeon *et al.*, 2017) from the rainfall event scale  
452 to that of several years. The long-term changes in rainfall intensity were also observed on dated sediment  
453 cores covering the Holocene (Barr et al., 2019). This impact has been rarely identified during the 20<sup>th</sup>  
454 century, however, due to a lack of sedimentary sequences recording storm deposits associated to intense  
455 rainfall events (Foucher et al., 2019a).

456 In addition to the concomitant oscillations observed both in sediment deposits and  
457 meteorological data, other oscillations, with a period of 6-11 years (Fig. 6), revealed by spectral analysis  
458 of MAR. These cyclicities were similar to the fluctuations exhibited by the North Atlantic Oscillation  
459 (NAO) with a period of 7-11 years (Hurrell, 1995). These oscillations also occurred with the same  
460 frequency as the land consolidation programmes (e.g. land consolidation operations were conducted on  
461 average every 9 years, SD 5 years). These additional wavelengths recorded in sedimentary sequences,  
462 although not observed in meteorological data, are probably inducible by an insufficient smoothing of  
463 the anthropogenic signal. As a consequence, the highest values of smoothed MAR were not correlated  
464 with the occurrence of more humid periods. Instead, they were correlated with the occurrence of more  
465 intensive agriculture activities in the Brosse catchment.

466 Finally, the poor correlation observed between rainfall data and high resolution smoothed MAR  
467 values during the 1960-2017 period is explainable by the potential errors made on sediment dating ( $\pm 1$   
468 year in 1963). This time gap does not allow comparison of the high resolution rainfall data (e.g. daily  
469 rainfall) with continuous records of sediment delivery. Other parameters, such as changes in primary

470 production, may increase the amount of material accumulated in the pond during summer despite the  
471 low rainfall levels generally observed during this period of the year. Quantifying the high resolution  
472 contribution of primary productivity on sediment dynamics remains a challenge and it could not be taken  
473 into account in the current research. Further methodological developments should improve of this  
474 relationship. Uncertainties associated with both core dating and estimations of the primary production  
475 can explain the discrepancies observed between the annual cyclicity associated with sediment delivery  
476 and rainfall.

477

478         Although erosion rates increased seven-fold in the Brosse catchment before the period 1950 to  
479 2017, reaching  $31.5 \text{ t km}^{-2} \text{ yr}^{-1}$  (SD  $2.5 \text{ t km}^{-2} \text{ yr}^{-1}$ ), they remain relatively low compared with those in  
480 other agricultural catchments of western Europe. For instance, in similar environments of France,  
481 sediment delivery of  $63 \text{ t km}^{-2} \text{ yr}^{-1}$  was measured in Brittany (catchment of  $4.5 \text{ km}^2$  dominated by  
482 grassland), (Vongvixay *et al.*, 2010). A rate of  $92 \text{ t km}^{-2} \text{ yr}^{-1}$  was also calculated based on sediment  
483 deposits collected in a pond draining a  $24 \text{ km}^2$  cultivated catchment of the Loire Basin (Foucher *et al.*,  
484 2014). Similar higher values were observed in the United Kingdom, with rates of  $90 \text{ t km}^{-2} \text{ yr}^{-1}$  recorded  
485 in the sedimentary sequences of the Kyre pool catchment ( $2.7 \text{ km}^2$  dominated by arable land) - (I. D. L.  
486 Foster *et al.*, 2003) and the Old Mild reservoir ( $1.5 \text{ km}^2$  dominated by rough grazing) - (Foster and  
487 Walling, 1994). In Belgium, Verstraeten and Poesen (2002) reported a wide range of values obtained  
488 from river gauging stations and analyses of pond deposits ranging from 60 to  $260 \text{ t km}^{-2} \text{ yr}^{-1}$ . The  
489 difference between values obtained in this research and those of other studies is explainable by the wide  
490 diversity of land cover, catchment sizes, soil properties or topography conditions between these different  
491 sites (e.g. de Vente *et al.*, 2007). Although they remain relatively low, however, these erosion rates are  
492 sufficient to lead to the rapid siltation of the Brosse pond.

493

## 494 5. Conclusions

495

496         Analysis of sediment accumulated in reservoirs provides a powerful technique for  
497 reconstructing the impact of climate and land use changes on soil erosion rates during the post-1950

498 period. Such a technique applied to an intensively cultivated lowland catchment in France produced  
499 answers to the research questions in this study. First, in the study area where soils were not highly  
500 sensitive to erosion, erosion rates increased seven-fold between 1928 and 2017. Soil erosion accelerated  
501 following agricultural intensification after World War II. It occurred simultaneously with an increase in  
502 the size of plots and a decrease of grassland/fallow land surfaces converted into cropland. Further,  
503 although cyclicities related to rainfall were evident when analysing these sediment deposits, the main  
504 factor controlling soil erosion is clearly attributable to land use change and agricultural intensification  
505 in the drainage area. This study demonstrated that these landscape modifications controlled the general  
506 trend in sediment supply over the post-1950 period, whereas rainfall controlled fluctuations in sediment  
507 delivery on shorter timescales. Such knowledge is of prime importance to implement effective  
508 mitigation programmes and reduce both on- and off-site deleterious impacts associated with soil  
509 erosion.

510

511

512

513

#### 514 References

515

516 Ahn, Y.S., Nakamura, F., Chun, K.W., 2010. Recent history of sediment dynamics in Lake Toro and  
517 applicability of <sup>210</sup>Pb dating in a highly disturbed catchment in northern Japan. *Geomorphology*.

518 <https://doi.org/10.1016/j.geomorph.2009.07.009>

519 Amundson, R., Berhe, A.A., Hopmans, J.W., Olson, C., Sztein, A.E., Sparks, D.L., 2015. Soil and  
520 human security in the 21st century. *Science* (80-. ). <https://doi.org/10.1126/science.1261071>

521 Appleby, P.G., Oldfield, F., 1978. The calculation of lead-210 dates assuming a constant rate of  
522 supply of unsupported <sup>210</sup>Pb to the sediment. *Catena* 5, 1–8. <https://doi.org/10.1016/S0341->

523 [8162\(78\)80002-2](https://doi.org/10.1016/S0341-8162(78)80002-2)

524 Bajard, M., Sabatier, P., David, F., Develle, A.-L., Reyss, J.-L., Fanget, B., Malet, E., Arnaud, D.,

525 Augustin, L., Crouzet, C., Poulénard, J., Arnaud, F., 2015. Erosion record in Lake La Thuile

526 sediments (Prealps, France): Evidence of montane landscape dynamics throughout the Holocene.  
527 The Holocene 26, 350–364. <https://doi.org/10.1177/0959683615609750>

528 Bakker, M.M., Govers, G., van Doorn, A., Quetier, F., Chouvardas, D., Rounsevell, M., 2008. The  
529 response of soil erosion and sediment export to land-use change in four areas of Europe: The  
530 importance of landscape pattern. *Geomorphology* 98, 213–226.  
531 <https://doi.org/10.1016/j.geomorph.2006.12.027>

532 Barr, C., Tibby, J., Leng, M.J., Tyler, J.J., Henderson, A.C.G., Overpeck, J.T., Simpson, G.L., Cole,  
533 J.E., Phipps, S.J., Marshall, J.C., McGregor, G.B., Hua, Q., McRobie, F.H., 2019. Holocene El  
534 Niño–Southern Oscillation variability reflected in subtropical Australian precipitation. *Sci. Rep.*  
535 <https://doi.org/10.1038/s41598-019-38626-3>

536 Ben Slimane, A., Raclot, D., Evrard, O., Sanaa, M., Lefèvre, I., Ahmadi, M., Tounsi, M., Rumpel, C.,  
537 Ben Mammou, A., Le Bissonnais, Y., 2013. Fingerprinting sediment sources in the outlet  
538 reservoir of a hilly cultivated catchment in Tunisia. *J. Soils Sediments*.  
539 <https://doi.org/10.1007/s11368-012-0642-6>

540 Boardman, J., Poesen, J., 2006. *Soil Erosion in Europe*. John Wiley & Sons, Ltd, Chichester, UK.  
541 <https://doi.org/10.1002/0470859202>

542 Borrelli, P., Robinson, D.A., Panagos, P., Lugato, E., Yang, J.E., Alewell, C., Wuepper, D.,  
543 Montanarella, L., Ballabio, C., 2020. Land use and climate change impacts on global soil erosion  
544 by water (2015-2070). *Proc. Natl. Acad. Sci.* 117, 21994–22001.  
545 <https://doi.org/10.1073/pnas.2001403117>

546 Boutin, J., Thomas, A., 1987. *Carte des sols de la région Centre au 1/50.000 – Feuille de Bléré.*  
547 *Chambre d’Agriculture d’Indre-et-Loire*.

548 Cambray, R.S., Playford, K., Carpenter, R.C., 1989. *Radioactive Fallout in Air and Rain: Results to*  
549 *the End of 1988*. Her Majesty’s Stn. Off, London Rep. AERE-.

550 Chaplot, V., Le Bissonnais, Y., 2000. Field measurements of interrill erosion under different slopes  
551 and plot sizes. *Earth Surf. Process. Landforms*. [https://doi.org/10.1002/\(SICI\)1096-](https://doi.org/10.1002/(SICI)1096-)  
552 [9837\(200002\)25:2<145::AID-ESP51>3.0.CO;2-3](https://doi.org/10.1002/(SICI)1096-9837(200002)25:2<145::AID-ESP51>3.0.CO;2-3)

553 Chartin, C., Evrard, O., Salvador-Blanes, S., Hirschberger, F., Van Oost, K., Lefèvre, I., Daroussin, J.,

554 Macaire, J.-J., 2013. Quantifying and modelling the impact of land consolidation and field  
555 borders on soil redistribution in agricultural landscapes (1954–2009). *CATENA* 110, 184–195.  
556 <https://doi.org/10.1016/j.catena.2013.06.006>

557 Croudace, I.W., Rothwell, R.G., 2015. Micro-XRF Studies of Sediment Cores: Applications of a non-  
558 destructive tool for the environmental sciences, *Developments in Paleoenvironmental Research*.  
559 <https://doi.org/10.1007/978-94-017-9849-5>

560 de Vente, J., Poesen, J., Arabkhedri, M., Verstraeten, G., 2007. The sediment delivery problem  
561 revisited. *Prog. Phys. Geogr.* <https://doi.org/10.1177/0309133307076485>

562 Dearing, J.A., 1991. Lake sediment records of erosional processes. *Hydrobiologia*.  
563 <https://doi.org/10.1007/BF00050938>

564 Dearing, J.A., Jones, R.T., 2003. Coupling temporal and spatial dimensions of global sediment flux  
565 through lake and marine sediment records. *Glob. Planet. Change* 39, 147–168.  
566 [https://doi.org/http://dx.doi.org/10.1016/S0921-8181\(03\)00022-5](https://doi.org/http://dx.doi.org/10.1016/S0921-8181(03)00022-5)

567 Evrard, O., Chaboche, P.-A., Ramon, R., Foucher, A., Laceby, J.P., 2020. A global review of sediment  
568 source fingerprinting research incorporating fallout radiocesium (<sup>137</sup>Cs). *Geomorphology*.  
569 <https://doi.org/10.1016/j.geomorph.2020.107103>

570 Evrard, O., Heitz, C., Liégeois, M., Boardman, J., Vandaele, K., Auzet, A. V., Van Wesemael, B.,  
571 2010. A comparison of management approaches to control muddy floods in central Belgium,  
572 northern France and southern England. *L. Degrad. Dev.* <https://doi.org/10.1002/ldr.1006>

573 Evrard, O., Laceby, J.P., Onda, Y., Wakiyama, Y., Jaegler, H., Lefèvre, I., 2016. Quantifying the  
574 dilution of the radiocesium contamination in Fukushima coastal river sediment (2011–2015). *Sci.*  
575 *Rep.* 6, 34828. <https://doi.org/10.1038/srep34828>

576 FAO, 2019. Soil erosion: the greatest challenge for sustainable soil management, Australian Surveyor.  
577 <https://doi.org/10.1080/00050326.1941.10437468>

578 FAO, 2006. World reference base for soil resources 2006: a framework for international classification,  
579 correlation and communication, *World Soil Resources Reports*. <https://doi.org/ISSN 0532-0488>

580 Foster, G.C., Dearing, J.A., Jones, R.T., Crook, D.S., Siddle, D.J., Harvey, A.M., James, P.A.,  
581 Appleby, P.G., Thompson, R., Nicholson, J., Loizeau, J.L., 2003. Meteorological and land use

582 controls on past and present hydro-geomorphic processes in the pre-alpine environment: An  
583 integrated lake-catchment study at the Petit Lac d'Annecy, France. *Hydrol. Process.*  
584 <https://doi.org/10.1002/hyp.1387>

585 Foster, I.D.L., Chapman, A.S., Hodgkinson, R.M., Jones, A.R., Lees, J.A., Turner, S.E., Scott, M.,  
586 2003. Changing suspended sediment and particulate phosphorus loads and pathways in  
587 underdrained lowland agricultural catchments; Herefordshire and Worcestershire, U.K., in: *The*  
588 *Interactions between Sediments and Water*. [https://doi.org/10.1007/978-94-017-3366-3\\_17](https://doi.org/10.1007/978-94-017-3366-3_17)

589 Foster, I.D.L., Collins, A.L., Naden, P.S., Sear, D.A., Jones, J.I., Zhang, Y., 2011. The potential for  
590 paleolimnology to determine historic sediment delivery to rivers. *J. Paleolimnol.*  
591 <https://doi.org/10.1007/s10933-011-9498-9>

592 Foster, I.D.L., Walling, D.E., 1994. Using reservoir deposits to reconstruct changing sediment yields  
593 and sources in the catchment of the Old Mill Reservoir, South Devon, UK, Over the past 50  
594 years. . *Hydrol. Sci.* 347–368.

595 Foucher, A., Evrard, O., Cerdan, O., Chabert, C., Lecompte, F., Lefèvre, I., Vandromme, R.,  
596 Salvador- Blanes, S., 2019a. A quick and low- cost technique to identify layers associated with  
597 heavy rainfall in sediment archives during the Anthropocene. *Sedimentology*.  
598 <https://doi.org/10.1111/sed.12650>

599 Foucher, A., Evrard, O., Chabert, C., Cerdan, O., Lefèvre, I., Vandromme, R., Salvador-Blanes, S.,  
600 2019b. Erosional response to land abandonment in rural areas of Western Europe during the  
601 Anthropocene: A case study in the Massif-Central, France. *Agric. Ecosyst. Environ.* 284,  
602 106582. <https://doi.org/10.1016/j.agee.2019.106582>

603 Foucher, A., Evrard, O., Huon, S., Curie, F., Lefèvre, I., Vaury, V., Cerdan, O., Vandromme, R.,  
604 Salvador-Blanes, S., 2020. Regional trends in eutrophication across the Loire river basin during  
605 the 20th century based on multi-proxy paleolimnological reconstructions. *Agric. Ecosyst.*  
606 *Environ.* 301, 107065. <https://doi.org/10.1016/j.agee.2020.107065>

607 Foucher, A., Salvador-Blanes, S., Evrard, O., Simonneau, A., Chapron, E., Courp, T., Cerdan, O.,  
608 Lefèvre, I., Adriaensen, H., Lecompte, F., Desmet, M., 2014. Increase in soil erosion after  
609 agricultural intensification: Evidence from a lowland basin in France. *Anthropocene* 7, 30–41.

610 <https://doi.org/10.1016/j.ancene.2015.02.001>

611 García-Ruiz, J.M., Beguería, S., Nadal-Romero, E., González-Hidalgo, J.C., Lana-Renault, N.,  
612 Sanjuán, Y., 2015. A meta-analysis of soil erosion rates across the world. *Geomorphology*.  
613 <https://doi.org/10.1016/j.geomorph.2015.03.008>

614 Gellis, A.C., Webb, R.M.T., McIntyre, S.C., Wolfe, W.J., 2006. Land-use effects on erosion, sediment  
615 yields, and reservoir sedimentation: A case study in the Lago Loíza Basin, Puerto Rico. *Phys.*  
616 *Geogr.* <https://doi.org/10.2747/0272-3646.27.1.39>

617 Giguët-Covex, C., Pansu, J., Arnaud, F., Rey, P.J., Griggo, C., Gielly, L., Domaizon, I., Coissac, E.,  
618 David, F., Choler, P., Poulénard, J., Taberlet, P., 2014. Long livestock farming history and  
619 human landscape shaping revealed by lake sediment DNA. *Nat. Commun.*  
620 <https://doi.org/10.1038/ncomms4211>

621 Grangeon, T., Manière, L., Foucher, A., Vandromme, R., Cerdan, O., Evrard, O., Pene-Galland, I.,  
622 Salvador-Blanes, S., 2017. Hydro-sedimentary dynamics of a drained agricultural headwater  
623 catchment: A nested monitoring approach. *Vadose Zo. J.* 16.  
624 <https://doi.org/10.2136/vzj2017.05.0113>

625 Hammer, Ø., Harper, D.A.T., Ryan, P.D., 2001. PAST: Paleontological Statistics Software Package  
626 for Education and Data Analysis. *Palaeontol. Electron.* 4–9.

627 Heathcote, A.J., Filstrup, C.T., Downing, J.A., 2013. Watershed Sediment Losses to Lakes  
628 Accelerating Despite Agricultural Soil Conservation Efforts. *PLoS One* 8, e53554.  
629 <https://doi.org/10.1371/journal.pone.0053554>

630 Hurrell, J.W., 1995. Decadal trends in the North Atlantic oscillation: Regional temperatures and  
631 precipitation. *Science* (80- ). <https://doi.org/10.1126/science.269.5224.676>

632 Issaka, S., Ashraf, M.A., 2017. Impact of soil erosion and degradation on water quality: a review.  
633 *Geol. Ecol. Landscapes.* <https://doi.org/10.1080/24749508.2017.1301053>

634 Klein Goldewijk, K., Beusen, A., Doelman, J., Stehfest, E., 2016. New anthropogenic land use  
635 estimates for the Holocene; HYDE 3.2. *Earth Syst. Sci. Data Discuss.* 1–40.  
636 <https://doi.org/10.5194/essd-2016-58>

637 Maetens, W., Vanmaercke, M., Poesen, J., Jankauskas, B., Jankauskiene, G., Ionita, I., 2012. Effects

638 of land use on annual runoff and soil loss in Europe and the Mediterranean. *Prog. Phys. Geogr.*  
639 *Earth Environ.* 36, 599–653. <https://doi.org/10.1177/0309133312451303>

640 Mann, L., Tolbert, V., Cushman, J., 2002. Potential environmental effects of corn (*Zea mays* L.) stover  
641 removal with emphasis on soil organic matter and erosion. *Agric. Ecosyst. Environ.*  
642 [https://doi.org/10.1016/S0167-8809\(01\)00166-9](https://doi.org/10.1016/S0167-8809(01)00166-9)

643 Marković, D., Koch, M., 2005. Wavelet and scaling analysis of monthly precipitation extremes in  
644 Germany in the 20th century: Interannual to interdecadal oscillations and the North Atlantic  
645 Oscillation influence. *Water Resour. Res.* <https://doi.org/10.1029/2004WR003843>

646 Massa, C., Bichet, V., Gauthier, É., Perren, B.B., Mathieu, O., Petit, C., Monna, F., Giraudeau, J.,  
647 Losno, R., Richard, H., 2012. A 2500 year record of natural and anthropogenic soil erosion in  
648 South Greenland. *Quat. Sci. Rev.* 32, 119–130. <https://doi.org/10.1016/j.quascirev.2011.11.014>

649 Meyers, P.A., 1994. Preservation of elemental and isotopic source identification of sedimentary  
650 organic matter. *Chem. Geol.* [https://doi.org/10.1016/0009-2541\(94\)90059-0](https://doi.org/10.1016/0009-2541(94)90059-0)

651 Mitchell, T.D., Hulme, M., 1999. Predicting regional climate change: Living with uncertainty. *Prog.*  
652 *Phys. Geogr.* <https://doi.org/10.1191/030913399672023346>

653 NF ISO 10693, 1995. Qualité du sol - Détermination de la teneur en carbonate - Méthode  
654 volumétrique.

655 Poisvert, C., 2018. Analyse et modélisation des surplus azotés en France au cours du siècle dernier:  
656 Application aux échelles départementales et communales. Université de Tours.

657 Rasplus, L., Macaire, J.-J., Alcaydé, G., 1982. Carte géologique de Bléré au 1:5000. BRGM.

658 Robinson, D.A., Panagos, P., Borrelli, P., Jones, A., Montanarella, L., Tye, A., Obst, C.G., 2017. Soil  
659 natural capital in Europe; A framework for state and change assessment. *Sci. Rep.*  
660 <https://doi.org/10.1038/s41598-017-06819-3>

661 Römken, M.J.M., Helming, K., Prasad, S.N., 2002. Soil erosion under different rainfall intensities,  
662 surface roughness, and soil water regimes, in: *Catena*. <https://doi.org/10.1016/S0341->  
663 [8162\(01\)00161-8](https://doi.org/10.1016/S0341-8162(01)00161-8)

664 Sabatier, P., Mottes, C., Cottin, N., Evrard, O., Comte, I., Piot, C., Gay, B., Arnaud, F., Lefevre, I.,  
665 Develle, A.-L., Deffontaines, L., Plet, J., Lesueur-Jannoyer, M., Poulenard, J., 2021. Evidence of

666 Chlordecone Resurrection by Glyphosate in French West Indies. *Environ. Sci. Technol.*  
667 <https://doi.org/10.1021/acs.est.0c05207>

668 Schiefer, E., Petticrew, E.L., Immell, R., Hassan, M.A., Sonderegger, D.L., 2013. Land use and  
669 climate change impacts on lake sedimentation rates in western Canada. *Anthropocene* 3, 61–71.  
670 <https://doi.org/10.1016/j.ancene.2014.02.006>

671 Schneider, C.A., Rasband, W.S., Eliceiri, K.W., 2012. NIH Image to ImageJ: 25 years of image  
672 analysis. *Nat. Methods* 9, 671–675. <https://doi.org/10.1038/nmeth.2089>

673 Simonneau, A., Doyen, E., Chapron, E., Millet, L., Vannière, B., Di Giovanni, C., Bossard, N.,  
674 Tachikawa, K., Bard, E., Albéric, P., Desmet, M., Roux, G., Lajeunesse, P., Berger, J.F., Arnaud,  
675 F., 2013. Holocene land-use evolution and associated soil erosion in the French Prealps inferred  
676 from Lake Paladru sediments and archaeological evidences. *J. Archaeol. Sci.* 40, 1636.

677 St-Onge, G., Long, B.F., 2009. CAT-scan analysis of sedimentary sequences: An ultrahigh-resolution  
678 paleoclimatic tool. *Eng. Geol.* 103, 127–133. <https://doi.org/10.1016/j.enggeo.2008.06.016>

679 Vandromme, R., Cerdan, O., Gay, A., Foucher, A., Salvador-Blanes, S., Lendemain, V., Desmet, M.,  
680 2013. The VERSEAU - TRACKSED Project: origin of Loire River basin sediments. 8th Int.  
681 SedNet Conf. 2013.

682 Vanmaercke, M., Poesen, J., Verstraeten, G., de Vente, J., Ocakoglu, F., 2011. Sediment yield in  
683 Europe: Spatial patterns and scale dependency. *Geomorphology* 130, 142.

684 Verstraeten, G., Poesen, J., 2002. Using sediment deposits in small ponds to quantify sediment yield  
685 from small catchments: Possibilities and limitations. *Earth Surf. Process. Landforms.*  
686 <https://doi.org/10.1002/esp.439>

687 Verstraeten, G., Poesen, J., 2000. Estimating trap efficiency of small reservoirs and ponds: methods  
688 and implications for the assessment of sediment yield. *Prog. Phys. Geogr.* 24, 219–251.  
689 <https://doi.org/10.1191/030913300676742153>

690 Vongvixay, A., Grimaldi, C., Gascuel-Oudou, C., Laguionie, P., Faucheux, M., Gilliet, N., Mayet, M.,  
691 2010. Analysis of suspended sediment concentration and discharge relations to identify particle  
692 origins in small agricultural watersheds 337, 14–18.

693 Wantzen, K.M., 1998. Effects of siltation on benthic communities in clear water streams in Mato

694 Grosso, Brazil. SIL Proceedings, 1922-2010. <https://doi.org/10.1080/03680770.1995.11900900>

695 Warren, J., Gilbert, R.O., 1988. Statistical Methods for Environmental Pollution Monitoring.

696 Technometrics. <https://doi.org/10.2307/1270090>

697

698

699 Figures:

700

701 Fig. 1 - Location of the study site within the Loire River Basin – A) Bathymetric map of the Brosse  
702 Pond and core sampling locations (red points) - B) Detailed map of the Brosse catchment – comparison  
703 of plot distribution and main land uses between 1950 and 2010.

704

705 Fig. 2 - A) Evolution of the main land uses between 1950 and 2010 based on the analysis of aerial images  
706 and agricultural census data – B) Evolution of the plot size between 1950 and 2010 based on the analysis  
707 of aerial images

708

709 Fig. 3 - Age-depth model of core BR-05 based on  $^{210}\text{Pb}_{\text{ex}}$  Constant Rate Supply model. The model was  
710 validated with the identification of the  $^{137}\text{Cs}$  fallout peak.

711

712 Fig. 4 – Dry bulk density, water content, Bulk organic and minerogenic matter, Mass Accumulation  
713 Rate of minerogenic matter (MARmin) and organic matter (MARorg), Ca/Ti ratio measured by XRF  
714 correlated to TOC and C:N ratio in the BR-05 sediment archive collected in the Brosse Pond and  
715 covering the 1928-2017 period.

716

717 Fig. 5 – Volume of minerogenic and organic sediment accumulated in the Brosse Pond between 1925  
718 and 2017. Evolution of erosion rates estimated from the variation of sediment volume and the evolution  
719 of catchment surface (Erosion min correspond to the minimal erosion calculated with the minerogenic

720 MAR. Error bar corresponds to the maximal erosion calculated when taking into account the organic  
721 fraction). The grey lines correspond to the occurrence of land consolidation operations.

722

723 Fig. 6 – Spectral analysis of the daily rainfall recorded between 1960 and 2017 in the Brosse catchment  
724 (left) and spectral analysis of high resolution MAR estimated with the CT-scan between 1960 and 2017.  
725 Red dashed lines correspond to the 0.01 significant level.

726

727 Fig. S1 - Land use evolution in the Brosse catchment reconstructed in 1950, 1970, 1990 and 2010).  
728 Illustration of the delineation between two agricultural fields in the upper part of the Brosse catchment  
729 (picture taken in 2018).

730

Figure 1

[Click here to access/download;Figure;figure-1-r2.jpg](#)

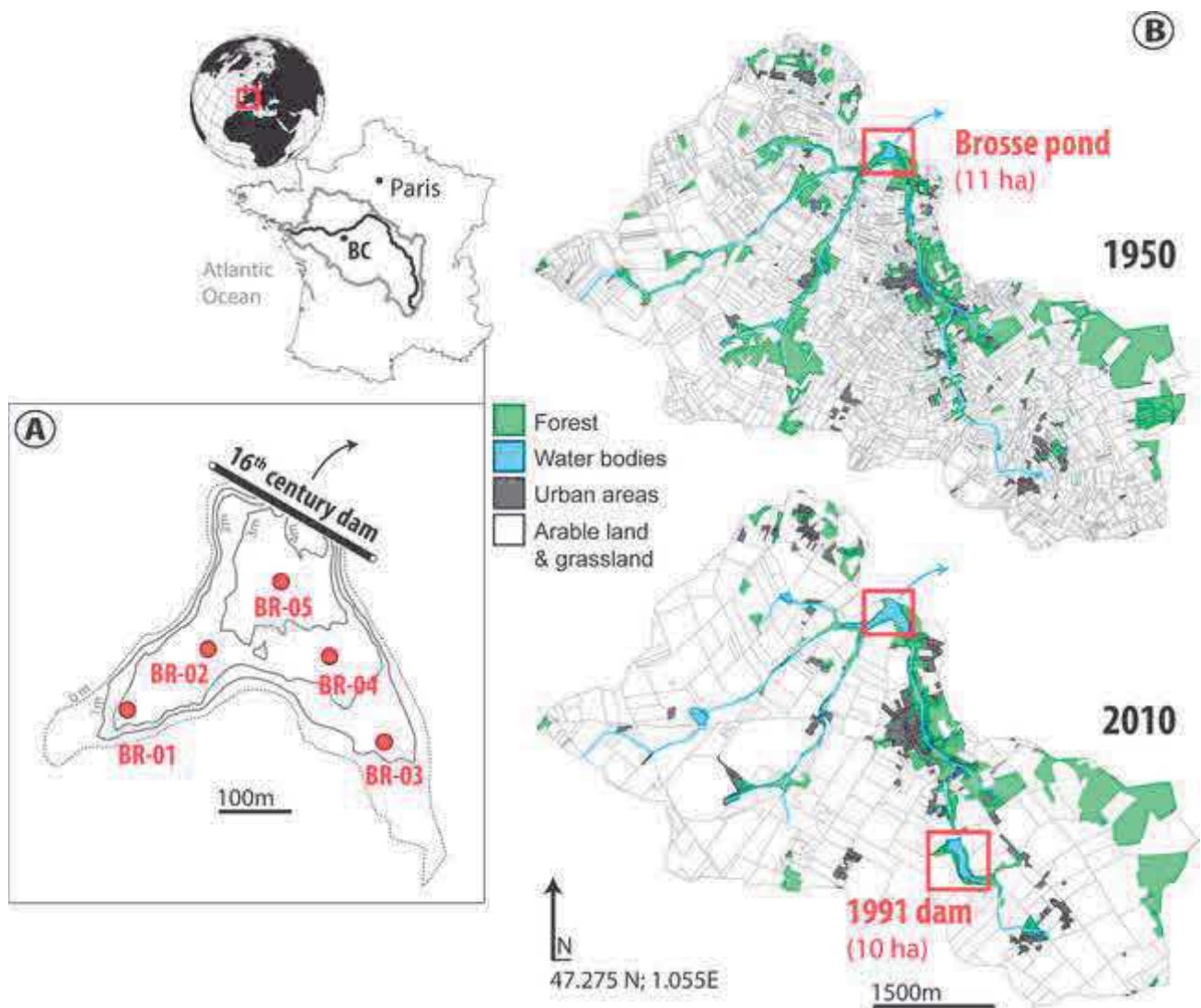


Figure 2

[Click here to access/download;Figure;figure 2 r2.jpg](#)

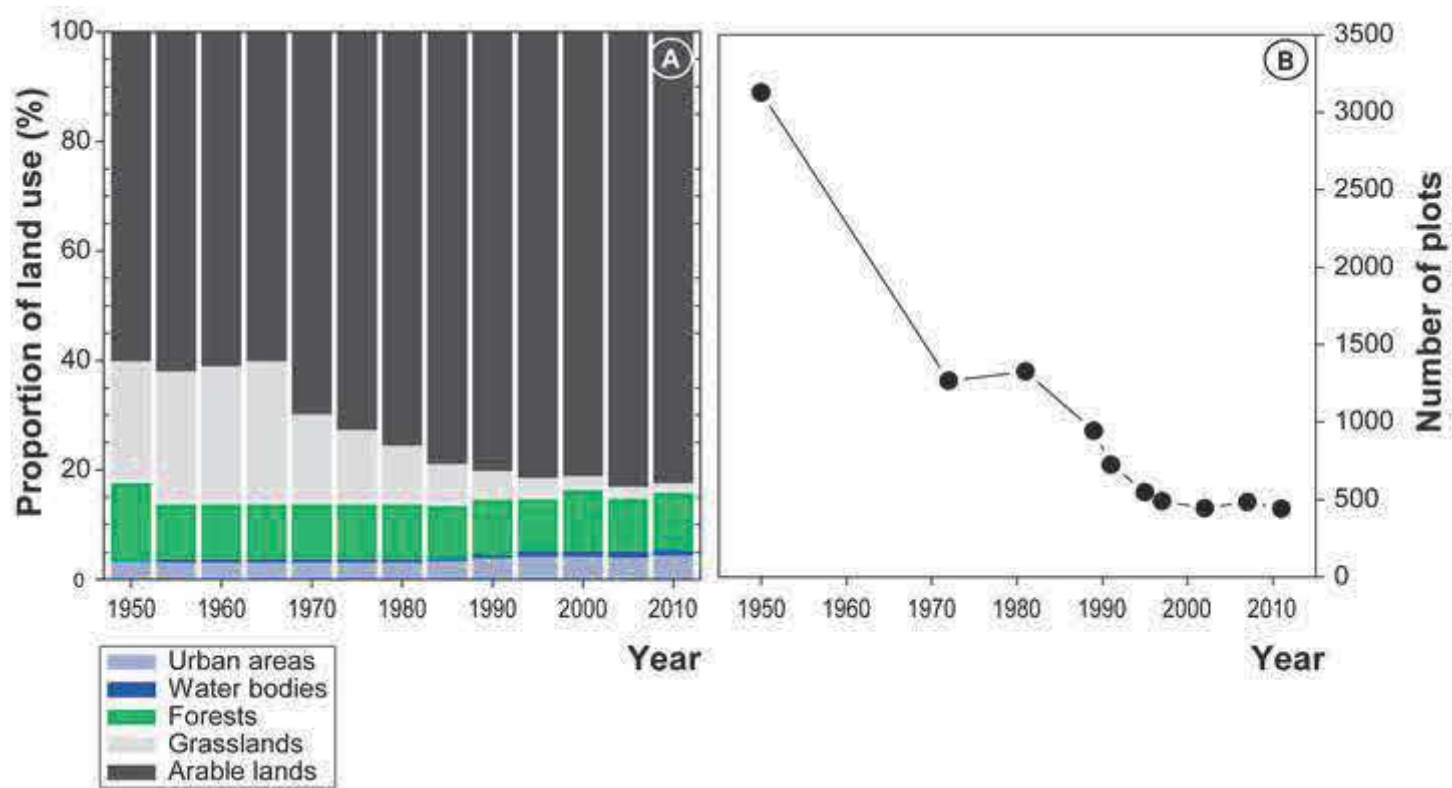


Figure 3

[Click here to access/download;Figure;figure3- r2.jpg](#)

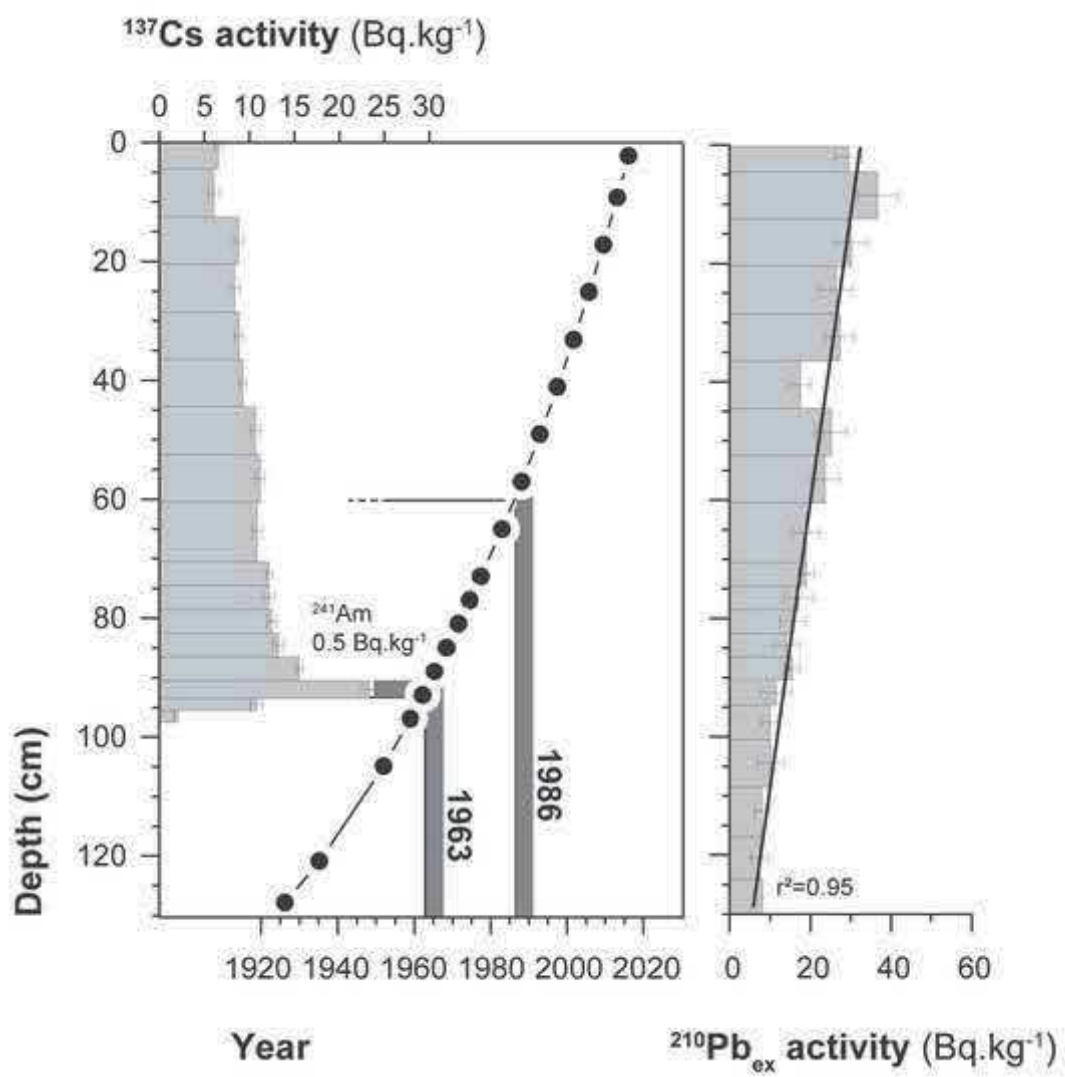


Figure 4

[Click here to access/download;Figure;figure 4 - r2.jpg](#)

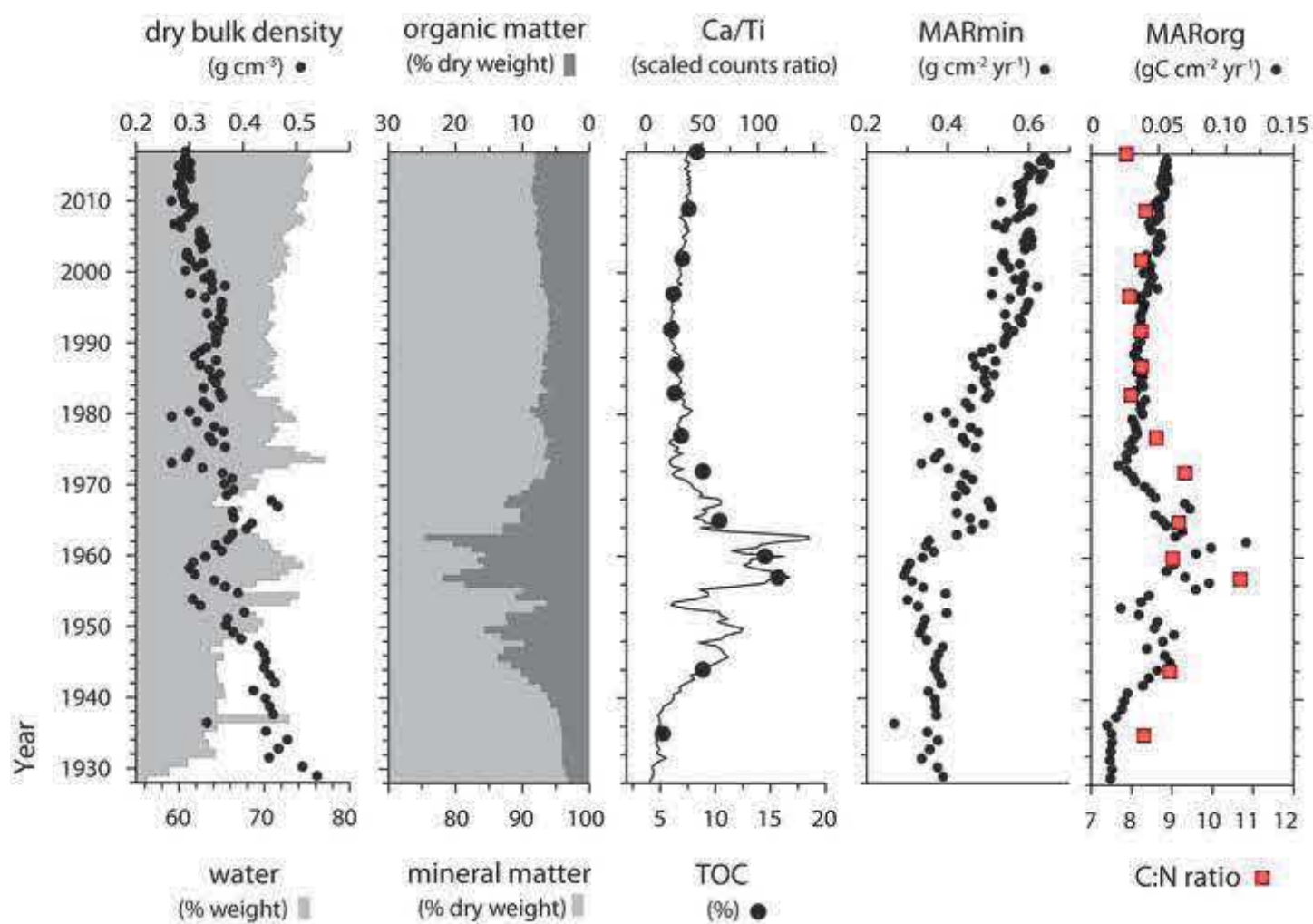


Figure 5

[Click here to access/download;Figure;figure 5 -r2.jpg](#)

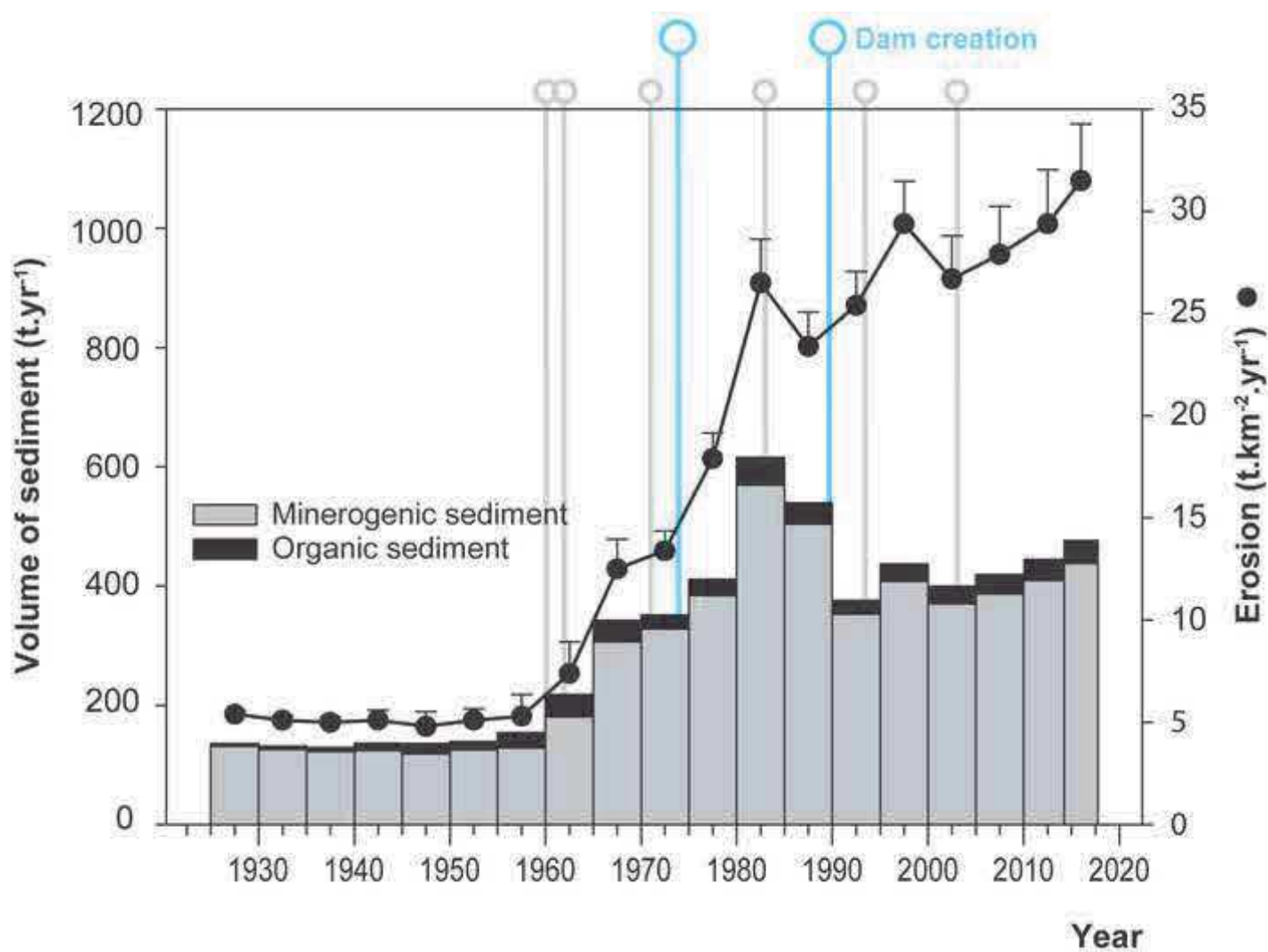
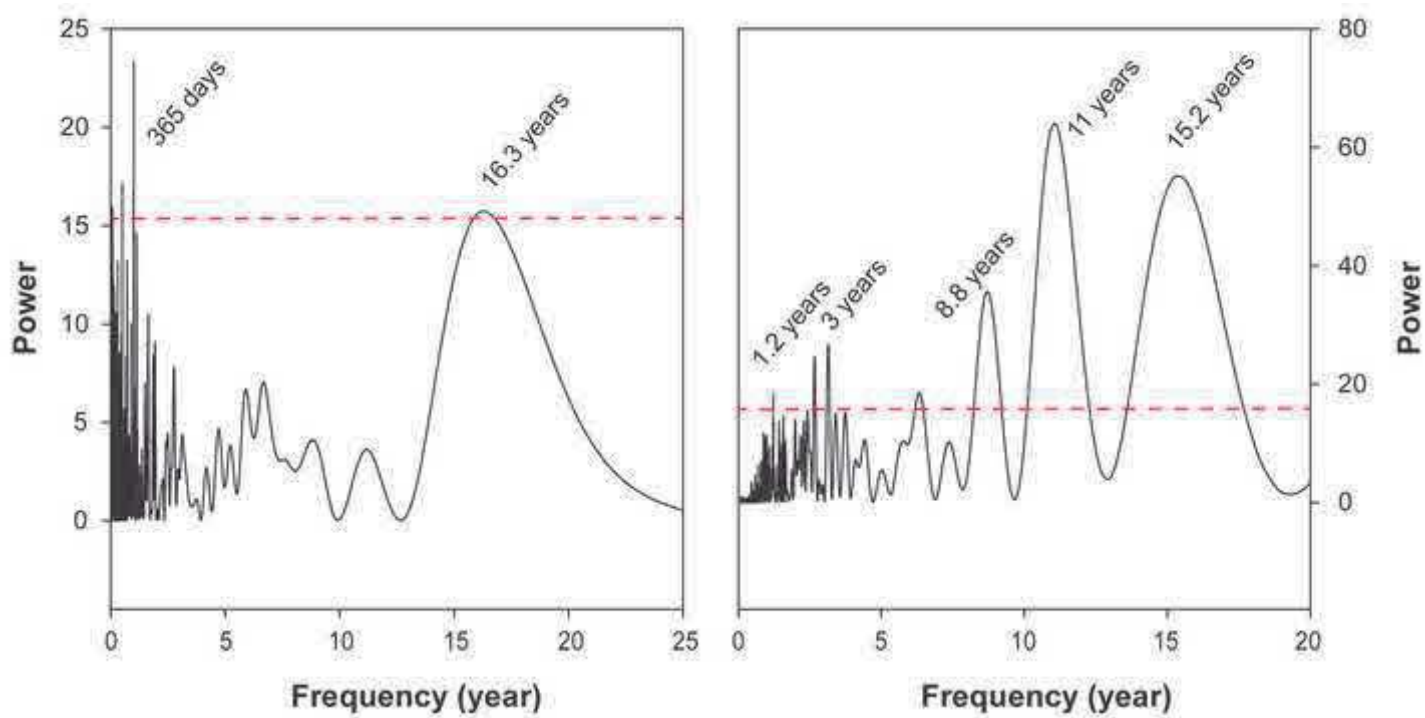


Figure 6

[Click here to access/download;Figure;figure 6.jpg](#)



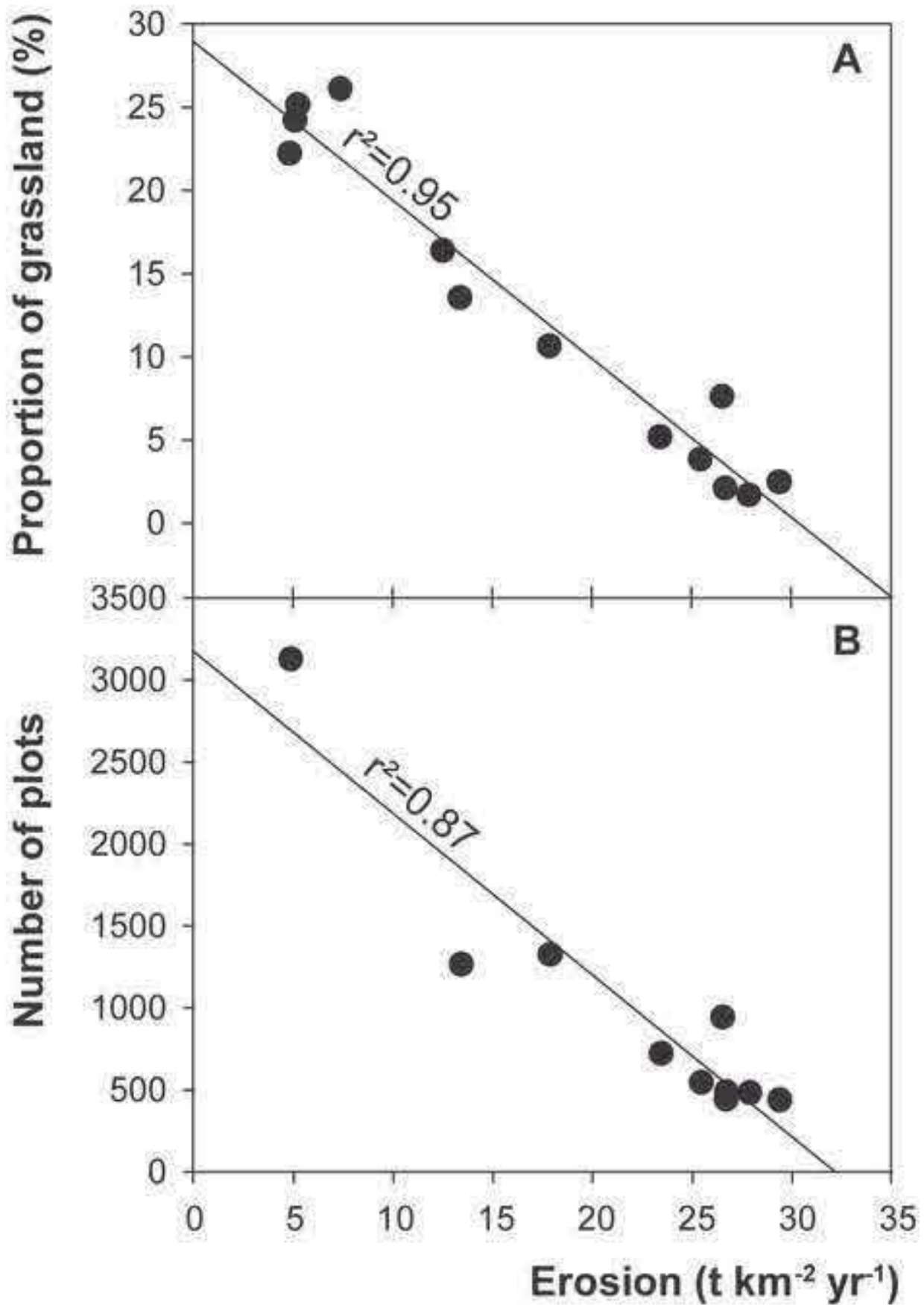
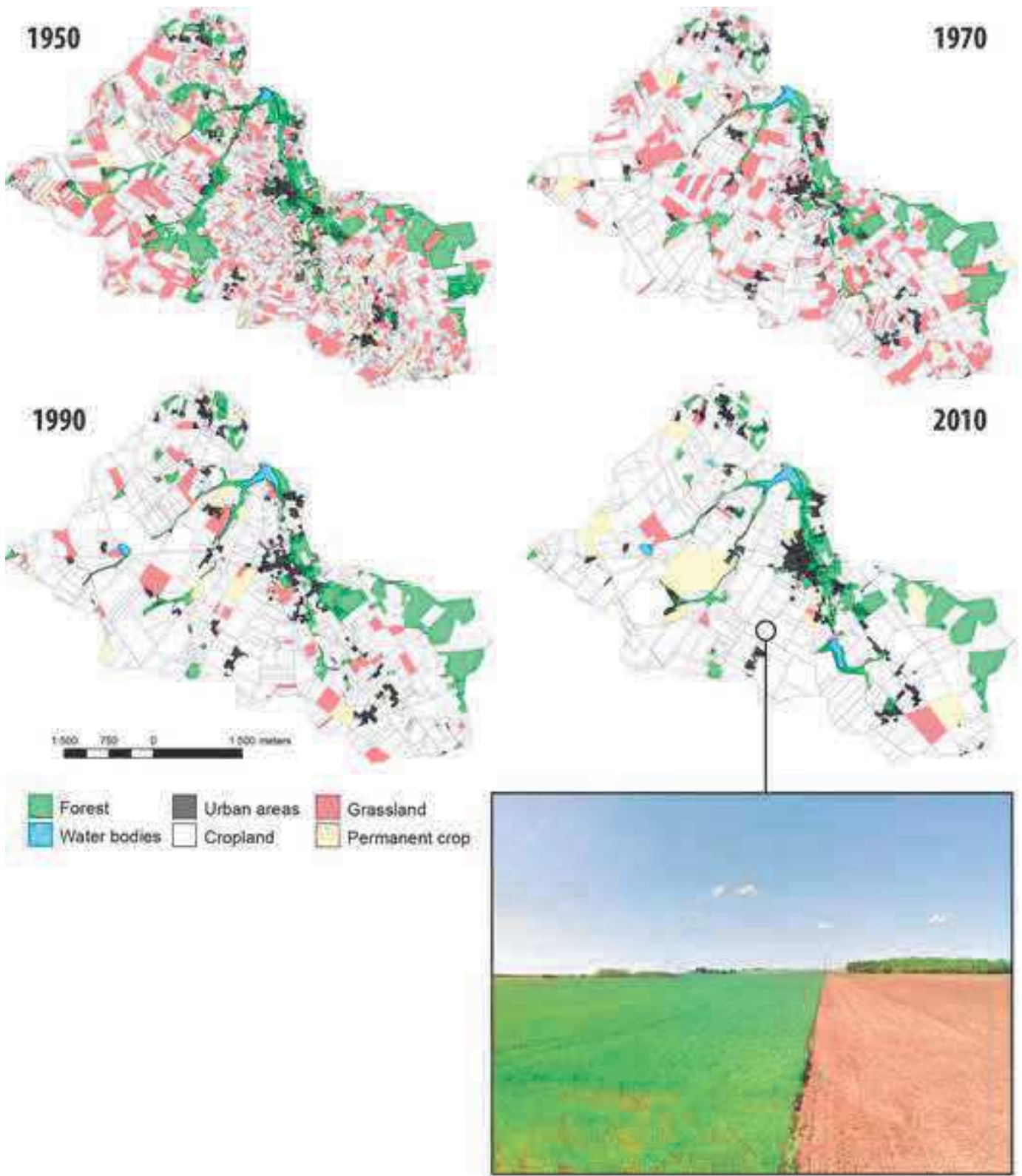


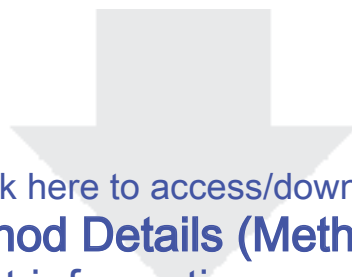
Figure S1: Land use evolution in the Brosse catchment reconstructed in 1950, 1970, 1990 and 2010). Illustration of the

[Click here to access/download;Figure;figure complémentaire anthropocene.jpg](#)

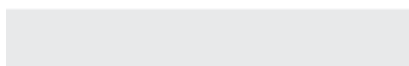
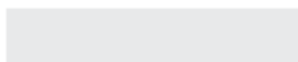


## Highlights

- Reconstruction of erosion rates in a lowland agricultural catchment during the 20<sup>th</sup> century
- Collection, dating and analysis of sediment cores in a pond draining this catchment
- Seven-fold increase of soil erosion rates between 1930 and 2017 ( $31.5 \text{ t km}^{-2} \text{ yr}^{-1}$ )
- Strong impact of land use change (grassland decline) on increasing erosion rates
- Occurrence of 1.2 years cyclicity was detected in cores and attributed to rainfall



Click here to access/download  
**Method Details (MethodX)**  
Supplement informations-methodX.docx



We confirm that there are no known conflicts of interest associated with this publication and there has been no significant financial support for this work that could have influenced its outcome.

We confirm that the manuscript has been read and approved by all named authors.

We confirm that the order of authors listed in the manuscript has been approved by all named authors.

Author's name	Affiliation
<u>Anthony Foucher</u>	<u>Laboratoire des Sciences du Climat et de l'Environnement, France</u>
<u>Olivier Evrard</u>	<u>Laboratoire des Sciences du Climat et de l'Environnement, France</u>
<u>Cerdan Olivier</u>	<u>BRGM, France</u>
<u>Clément Chabert</u>	<u>BRGM, France</u>
<u>Irène Lefèvre</u>	<u>Laboratoire des Sciences du Climat et de l'Environnement, France</u>
<u>Rosalie Vandromme</u>	<u>BRGM, France</u>
<u>Sébastien Salvador-Blanes</u>	<u>Université de Tours, France</u>

Conflict of Interest and Authorship Conformation Form

Please check the following as appropriate:

- All authors have participated in (a) conception and design, or analysis and interpretation of the data; (b) drafting the article or revising it critically for important intellectual content; and (c) approval of the final version.
- This manuscript has not been submitted to, nor is under review at, another journal or other publishing venue.
- The authors have no affiliation with any organization with a direct or indirect financial interest in the subject matter discussed in the manuscript
- The following authors have affiliations with organizations with direct or indirect financial interest in the subject matter discussed in the manuscript:

Author's name	Affiliation
<u>Anthony Foucher - Laboratoire des Sciences du Climat et de l'Environnement, France</u>	
<u>Olivier Evrard - Laboratoire des Sciences du Climat et de l'Environnement, France</u>	
<u>Cerdan Olivier – BRGM, France</u>	
<u>Clément Chabert – BRGM, France</u>	
<u>Irène Lefèvre - Laboratoire des Sciences du Climat et de l'Environnement, France</u>	
<u>Rosalie Vandromme – BRGM, France</u>	
<u>Sébastien Salvador-Blanes – Université de Tours, France</u>	